Data Repository of Paper doi# 10.1130/B31125.1, Geological Society of America Bulletin:

Constructing Forearc Architecture over Megathrust Seismic Cycles: Geological Snapshots from the Maule Earthquake Region, Chile

Felipe Aron[1,*,§], José Cembrano[2,3,4], Felipe Astudillo[5], Richard W. Allmendinger[1], Gloria Arancibia[2,4]

[1]*Department of Earth and Atmospheric Sciences, Cornell University, Ithaca, New York 14853, USA*

[2]*Departamento de Ingeniería Estructural y Geotécnica, Pontificia Universidad Católica de Chile, Vicuña Mackenna 4860, Macul, Santiago, Chile*

[3]*National Research Center for Integrated Natural Disasters Management (CIGIDEN), Vicuña Mackenna 4860, Macul, Santiago, Chile*

[4]*Centro de Excelencia en Geotermia de los Andes (CEGA, Fondap-Conicyt, 15090013), Plaza Ercilla 803, Santiago, Chile*

[5]*Departamento de Ciencias Geológicas, Universidad Católica del Norte, Avenida Angamos 0610, Antofagasta, Chile*

[*]E-mail: faa32@cornell.edu

[§]Current address: Department of Geological and Environmental Sciences, Stanford University, Stanford, California 94305

DR Section 1. Additional structural field examples of the O'Higgins study region

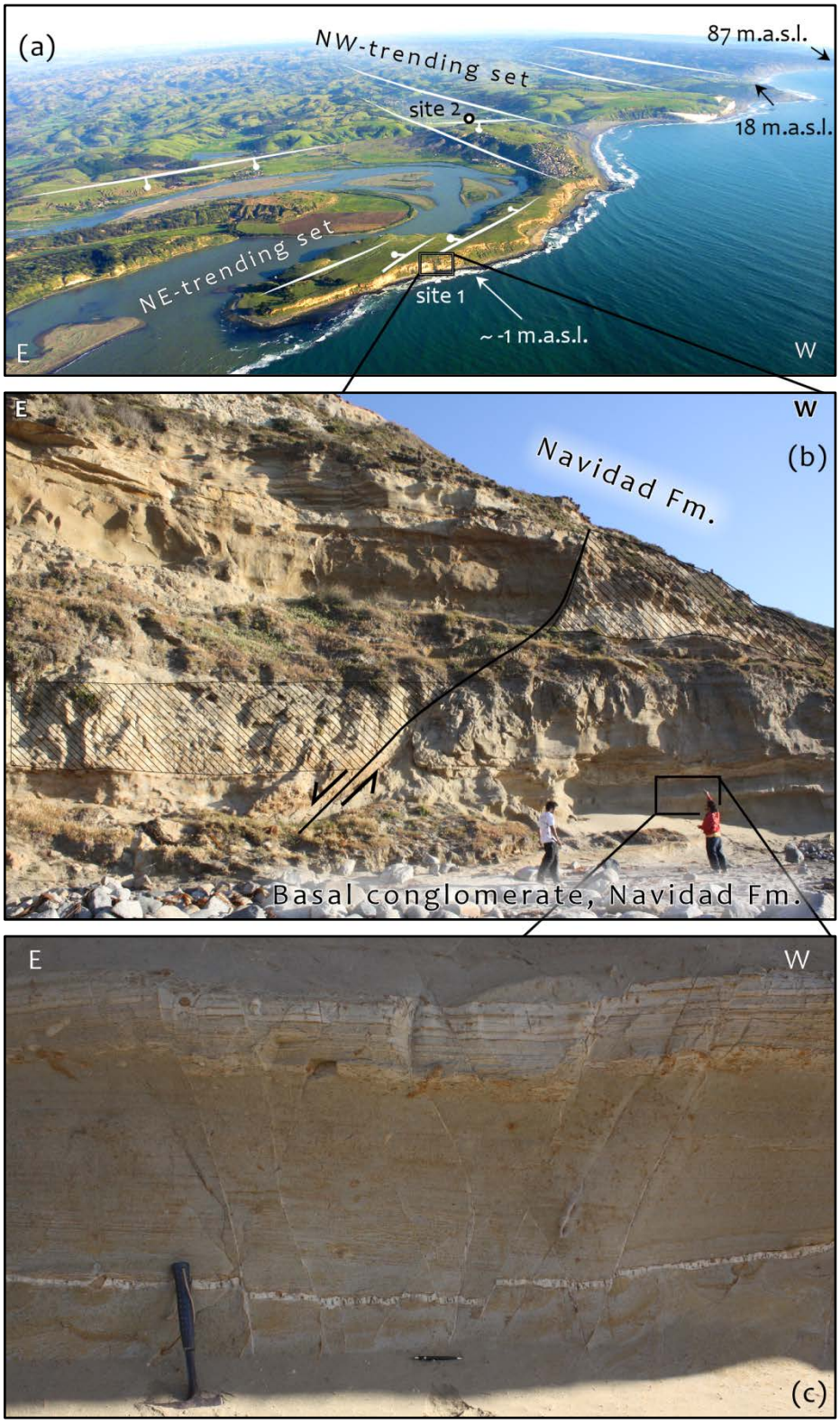

Figure DR1: (a) Aerial view looking south showing the 2 major, orthogonal fault sets affecting the northern portion of the O'Higgins region (Boca de Rapel-Matanzas domain of Fig. 2 and Section 4.1.1 in main manuscript). Locations of site 1 and site 2 are shown at the lower center (black box) and center of the picture (white dot). The NW-trending set of faults generates a flight of marine terraces to the south, offsetting both the morphologic, marine terraces and the sub-horizontal contact between the basement and the Navidad Fm., shown by the altitude numbers, along the coastal cliff. *Photo by Horacio Parragué*. (b) Color version of Fig. 3 in main manuscript. (c) Close up to minor subsidiary normal faults affecting the foot-wall (Fault 1b in Table 1).

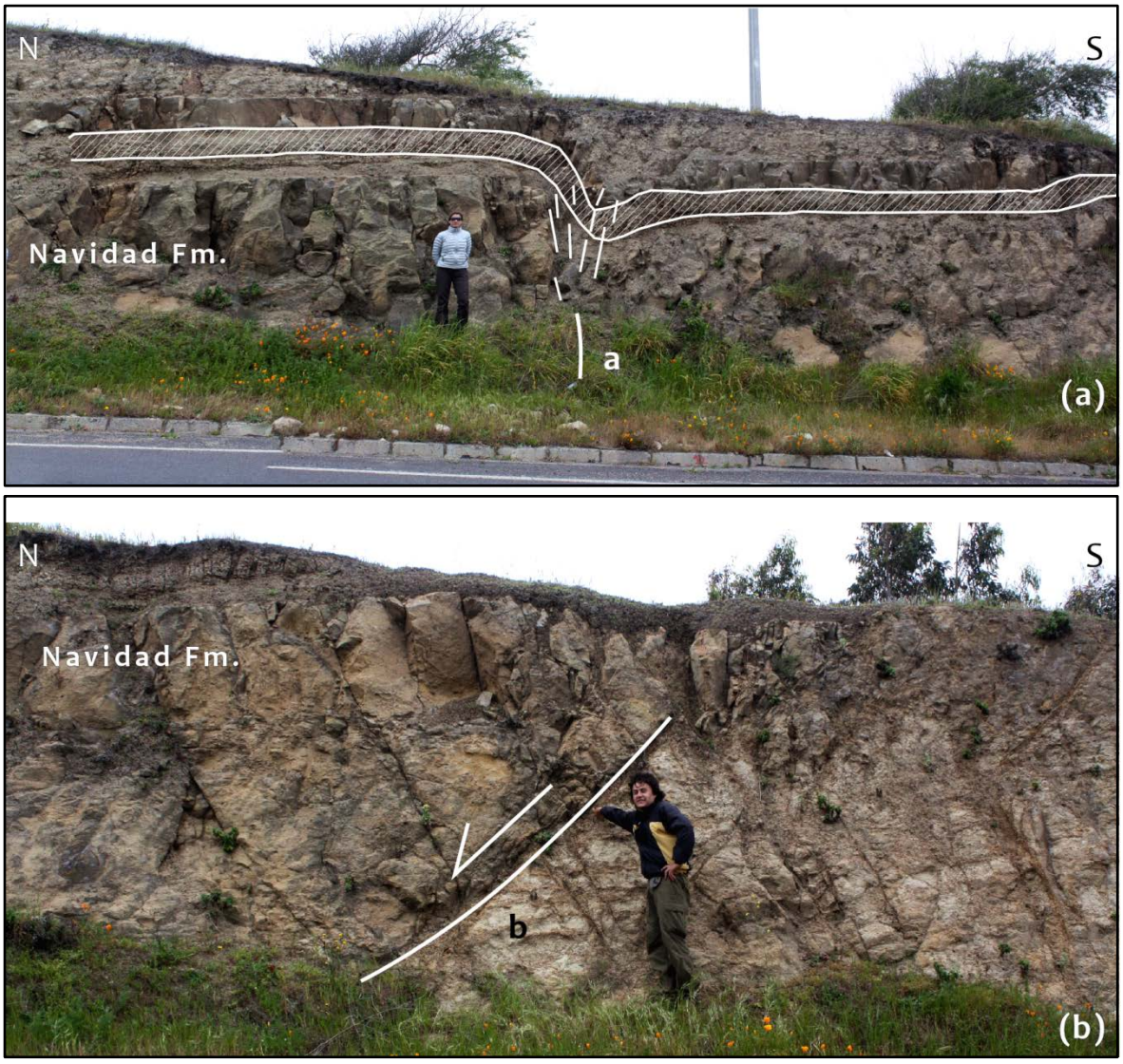

Figure DR2: Outcrop of normal faults “a” and “b” found in site 2 affecting the Navidad Fm. (Fig. 2, Table 1 and Section 4.1.1 in main manuscript).

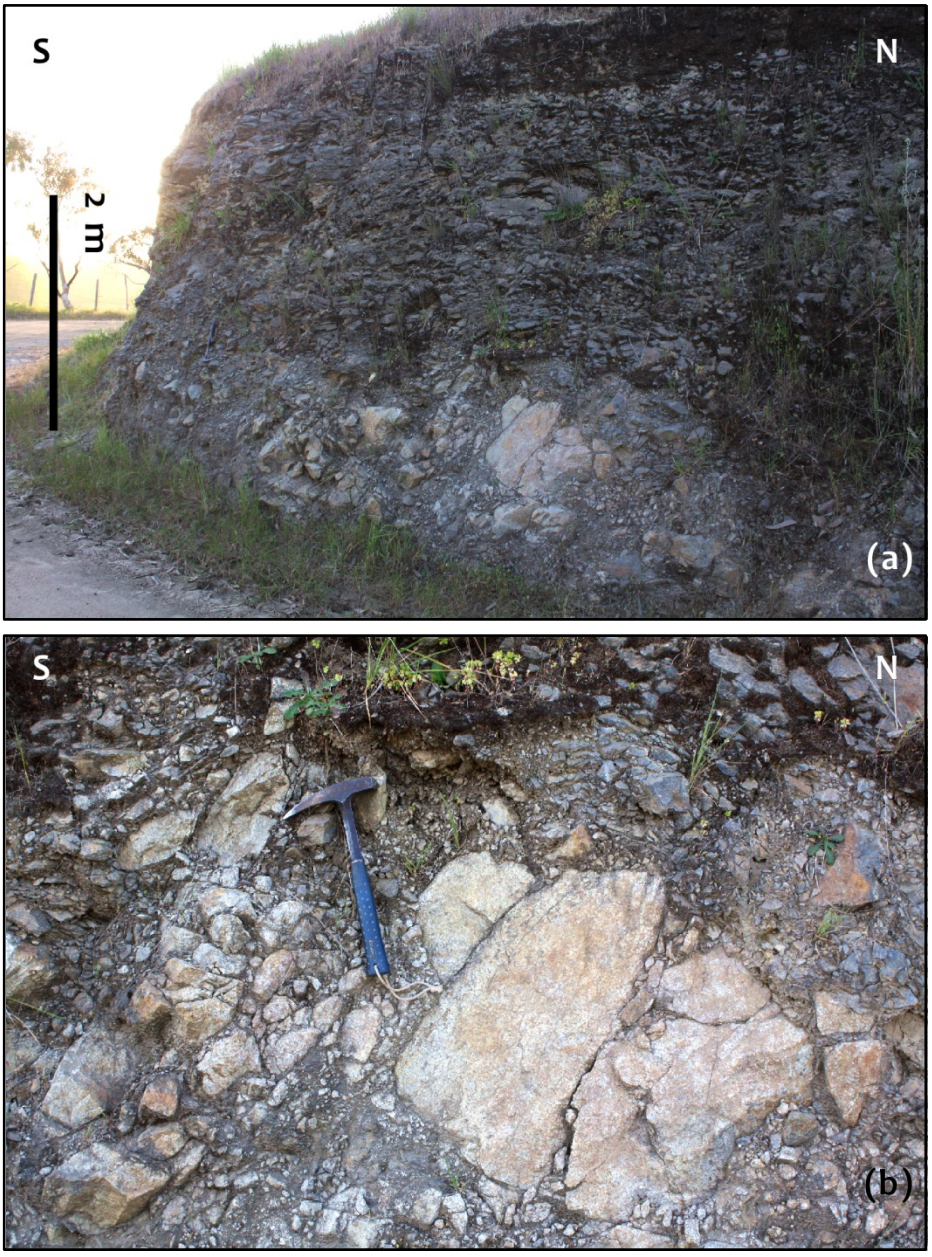

Figure DR3: (a) Outcrop of fault breccia described in site 3 which may mark the intersection of two orthogonal fault systems (NE- and NW-trending structures). (b) Close up to fault breccia. See Fig. 2, Table 1 and Section 4.1.2 in main manuscript.

Figure DR4: (a) Aerial view looking NNW of the Topocalma fault described in site 4 (Fig. 2, Table 1 and Section 4.1.2 in main manuscript). (b) Color version of Figure 4 in main manuscript. The top of the hill behind the fresh fault plane of the structure is about 100 m high. *Photos by Horacio Parragué.*

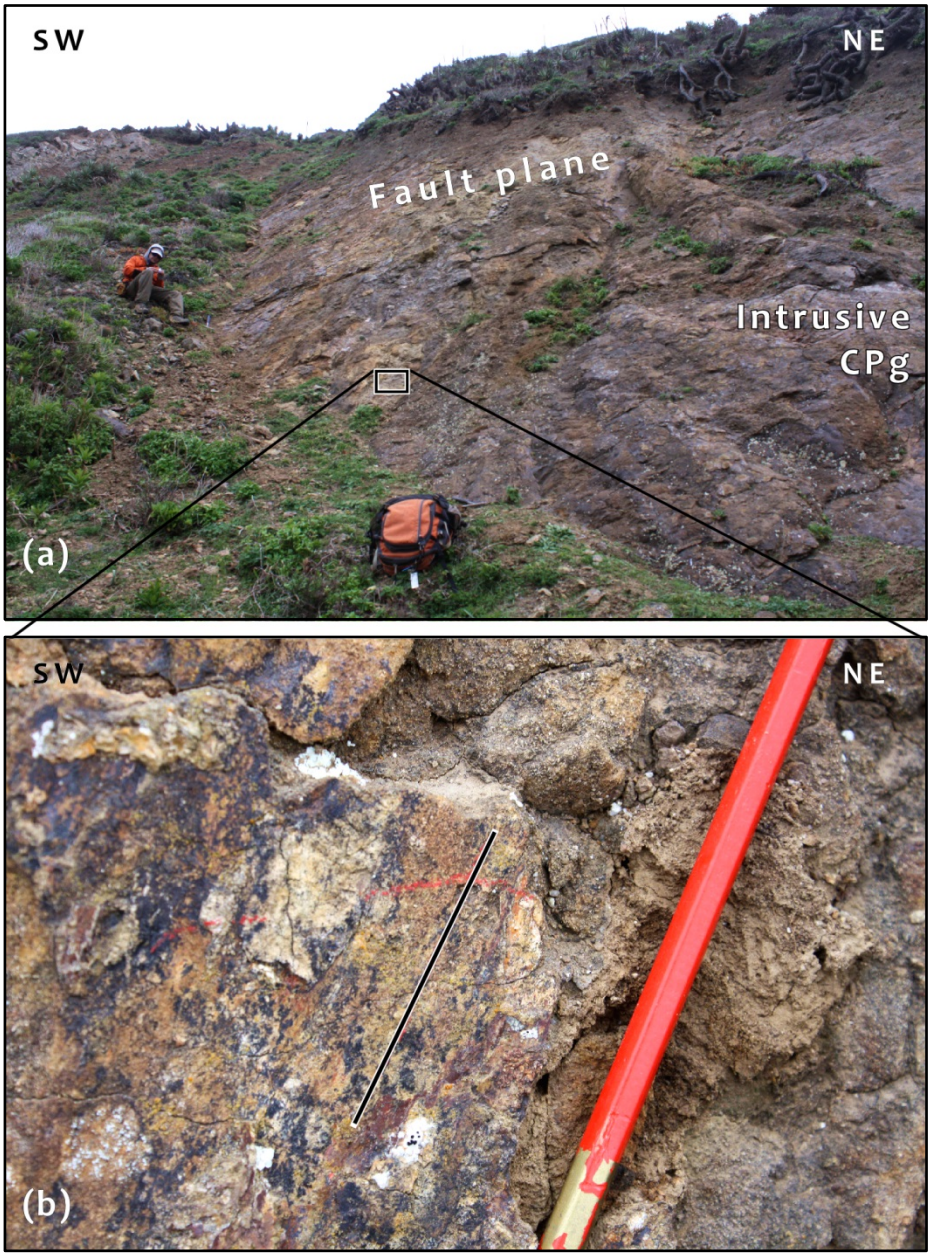

Figure DR5: (a) Outcrop of the Topocalma fault plane (Fig. 2, Table 1 and Section 4.1.2 in main manuscript; see also Figures 4 and DR4 for reference). (b) Close up showing slickensides on the fresh fault plane.

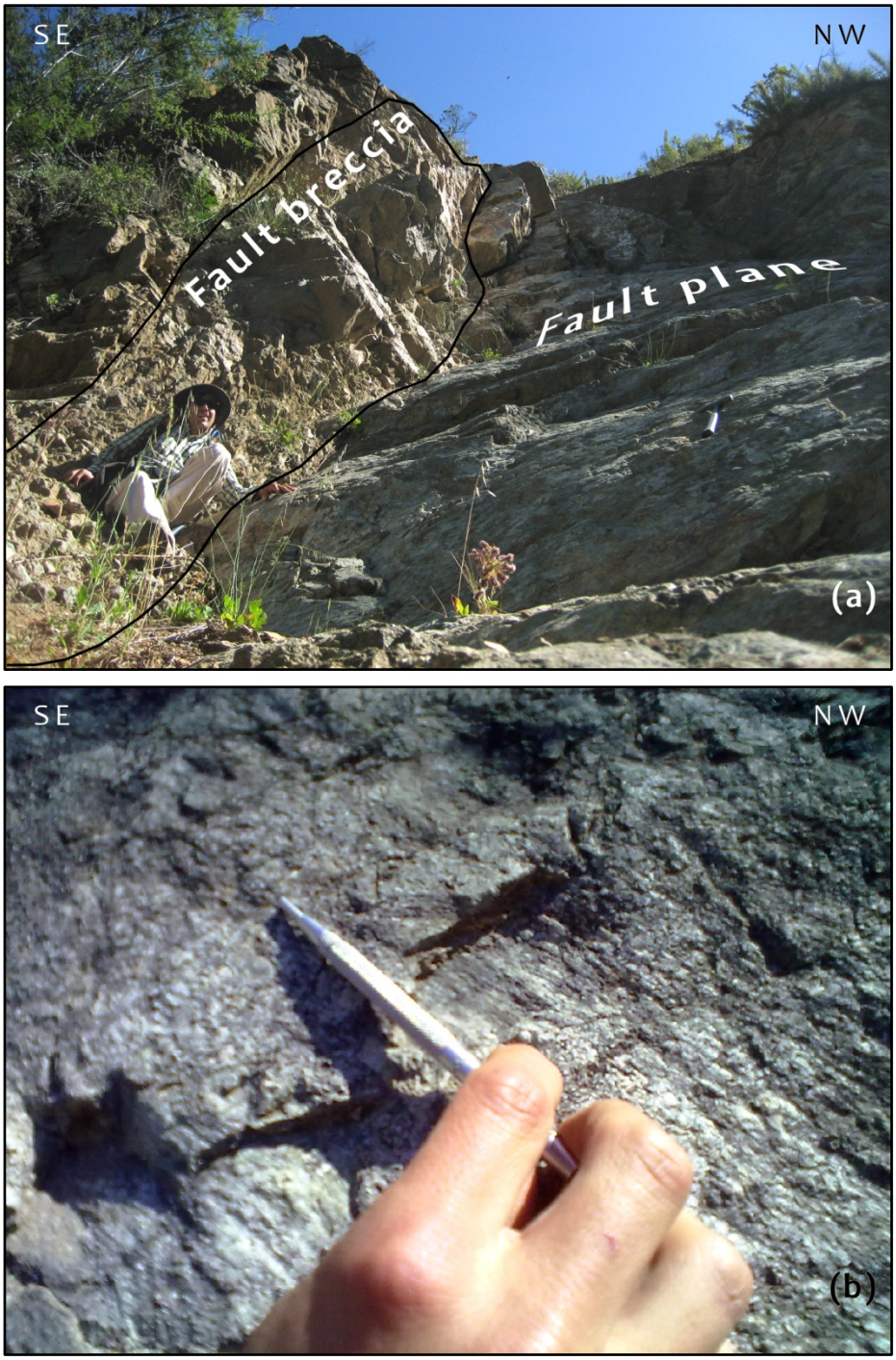

Figure DR6: (a) Outcrop of the Quebrada Honda fault described in site 5 (Fig. 2, Table 1 and Section 4.1.2 in main manuscript). (a) Color version of Figure 5, main manuscript. (b) Close up to striated plane.

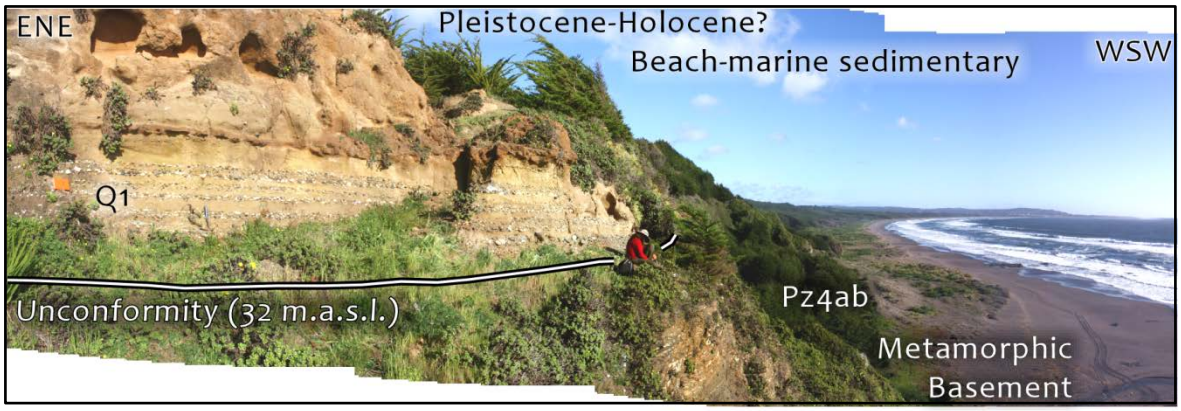

Figure DR7: Color version of Figure 7b in main manuscript.

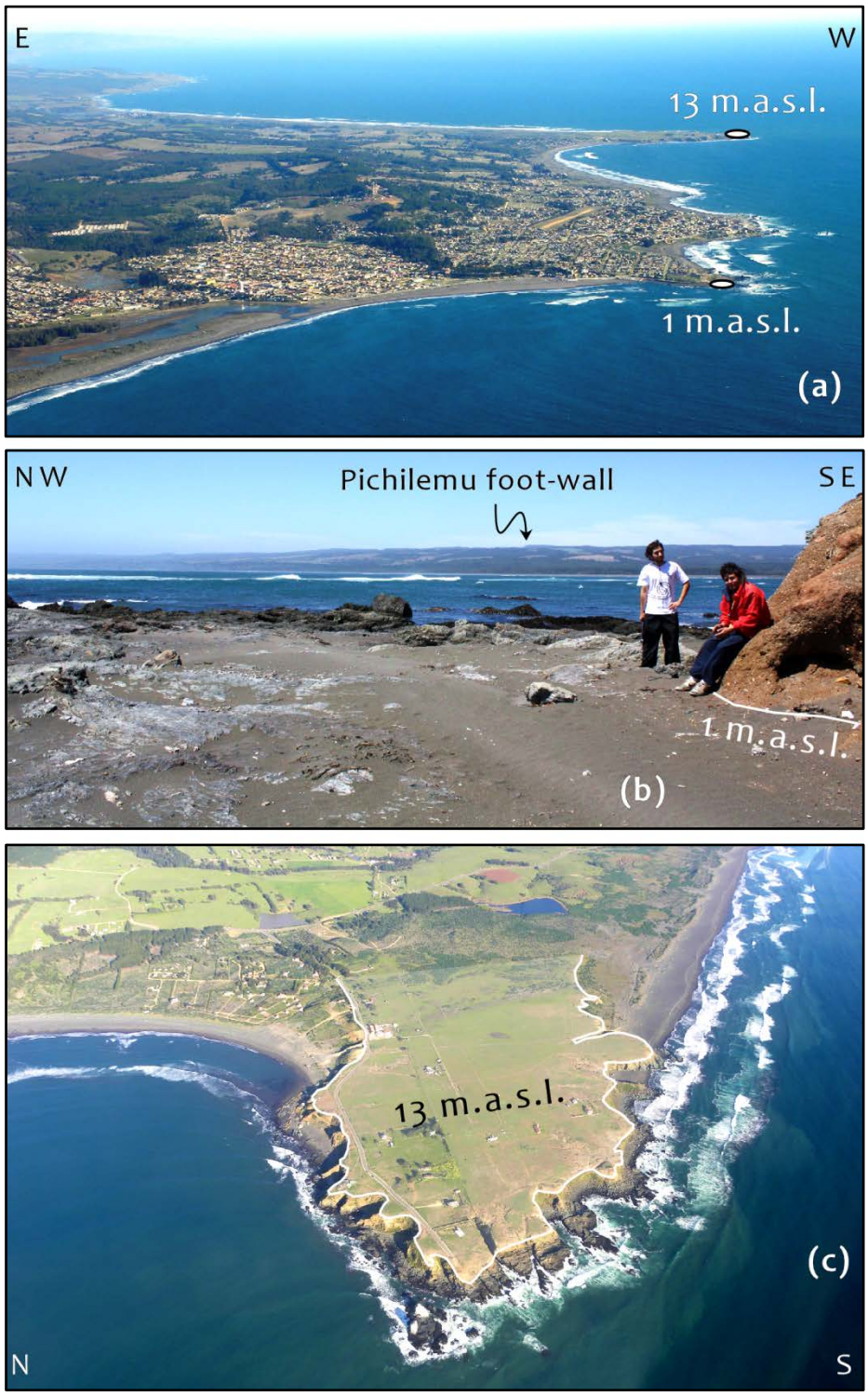

Figure DR8: (a) Aerial view looking south, away from the structure, of the hanging-wall of the Pichilemu fault showing a gentle rollover towards the fault, depicted by the Quaternary paleo-abrasion platform as described in Section 4.1.3 in main manuscript (see Fig. 7a). *Photo by Horacio Parragué.* (b) Outcrop of the contact lying at 1 meter above sea level. Note the foot-wall of the structure in the background across the bay. (c) Aerial view looking straight down to the terrace where the contact lies at 13 m.a.s.l. *Photo by Horacio Parragué.*

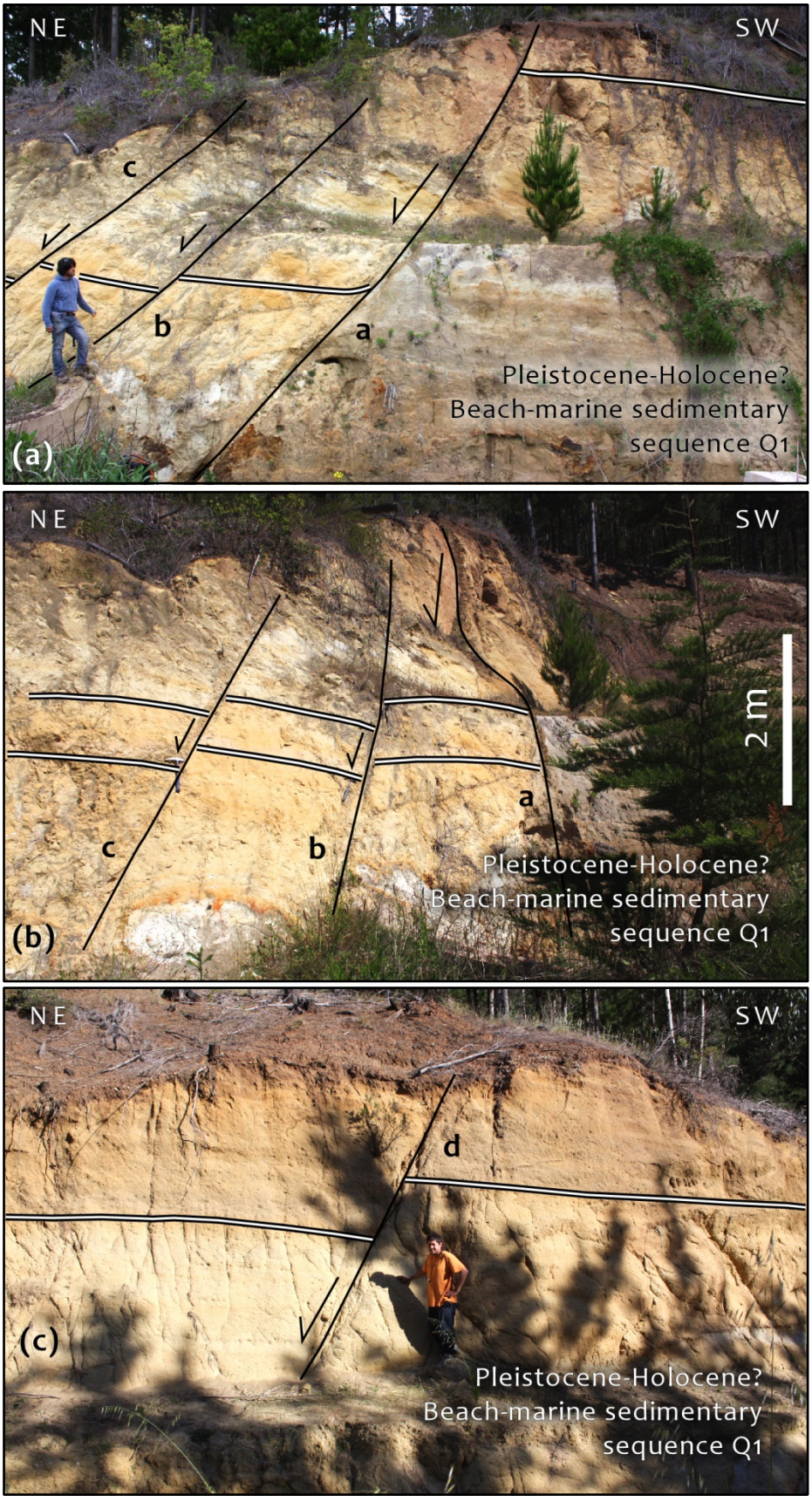

Figure DR9: Outcrop of normal faults described in site 6 (Fig. 2, Table 1 and Section 4.1.3 in main manuscript). These structures cut the foot-wall of the Pichilemu fault, close to the trace, and are antithetic to the main structure. They affect the Quaternary sedimentary rocks evidencing young, probably active deformation. Fault “d” showed in picture (c) cuts the foot-wall of fault “a” and is located about 150 m away from that structure.

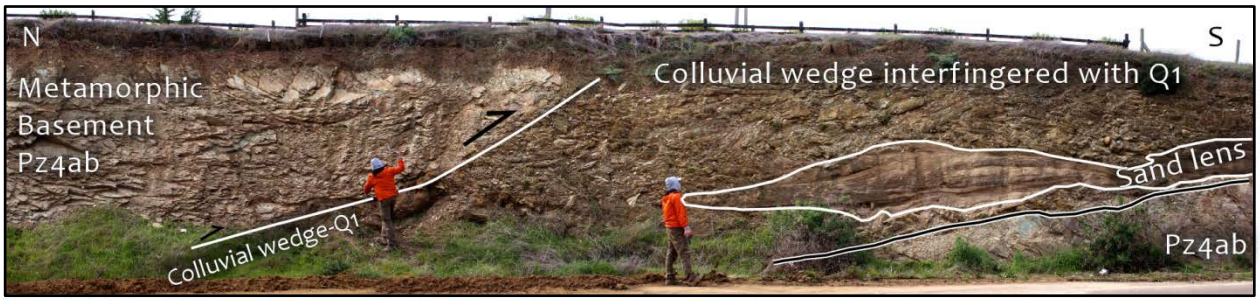

Figure DR10: Outcrop of reverse fault affecting metamorphic basement and Quaternary sedimentary rocks as described in site 8 (Fig. 2, Table 1 and Section 4.1.4 in main manuscript). Note the colluvial wedge of basement material mixed with sand in the foot-wall in front of the fault.

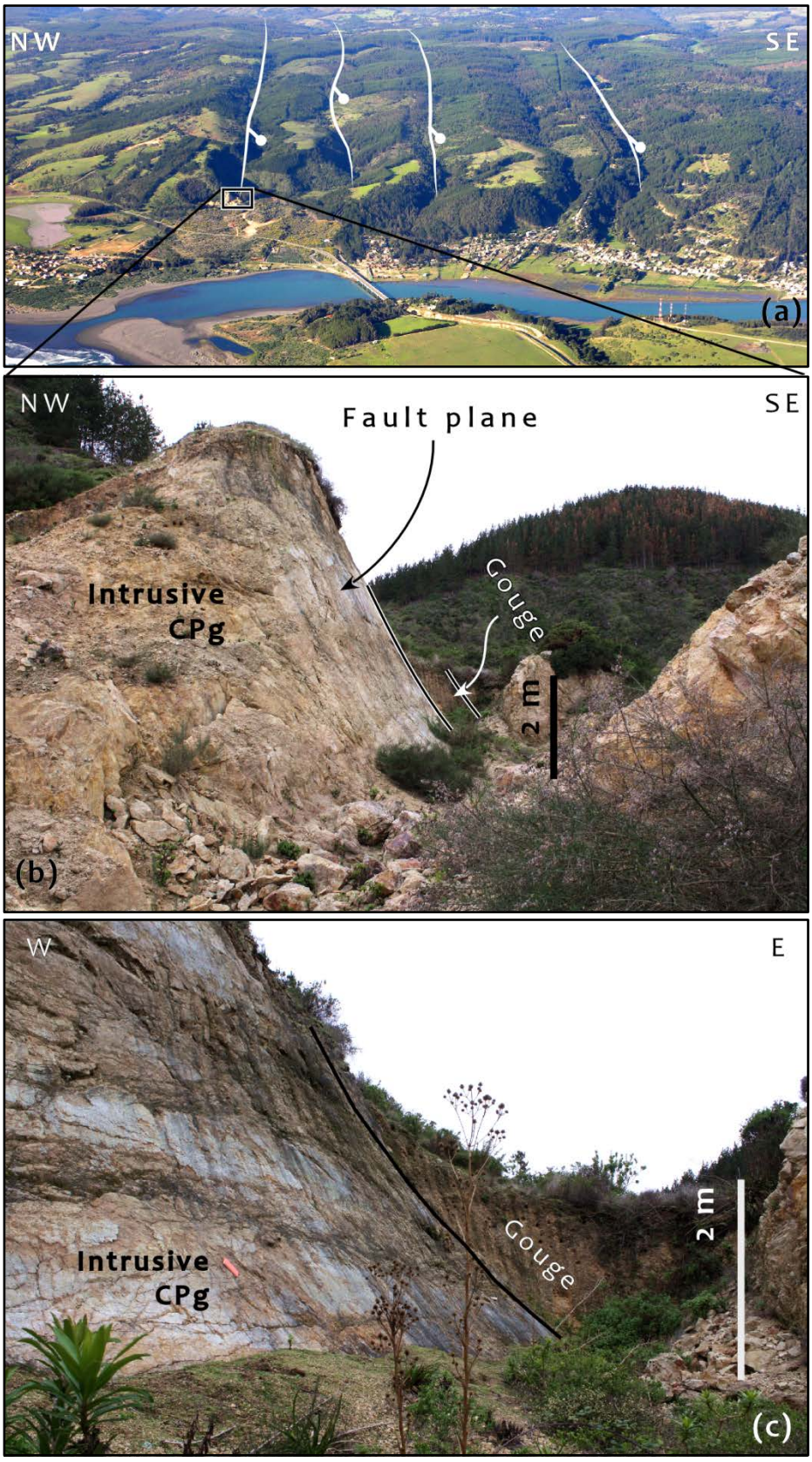

Figure DR11: (a) and (b) are color versions of Figure 8 in main manuscript. (c) Close up to fault plane shown in (b). *Aerial view by Horacio Parragué.*

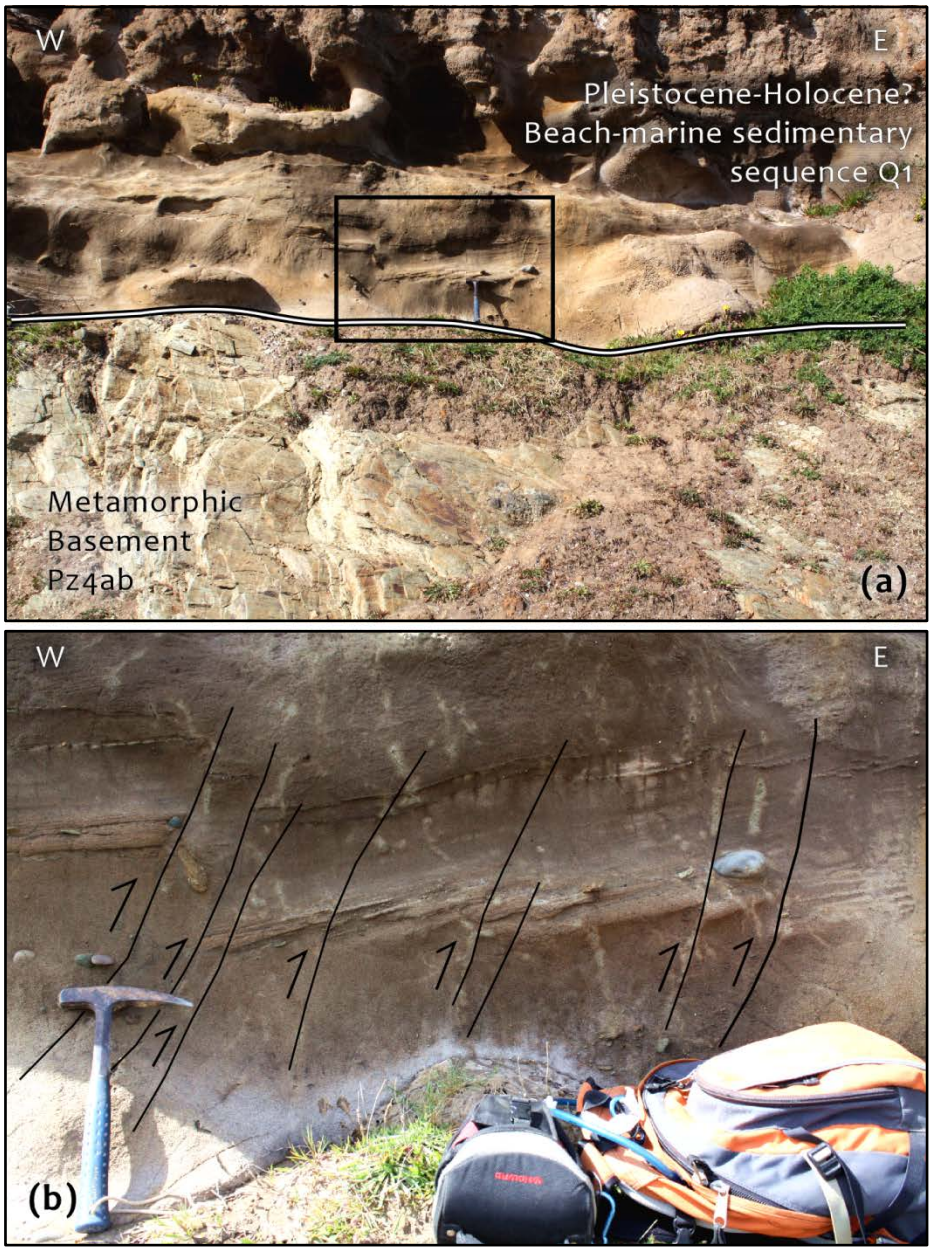

Figure DR12: Minor centimeter-scale reverse faults affecting the Quaternary sedimentary sequences found at site 10 (Fig. 2, Table 1 and Section 4.1.4 in main manuscript).

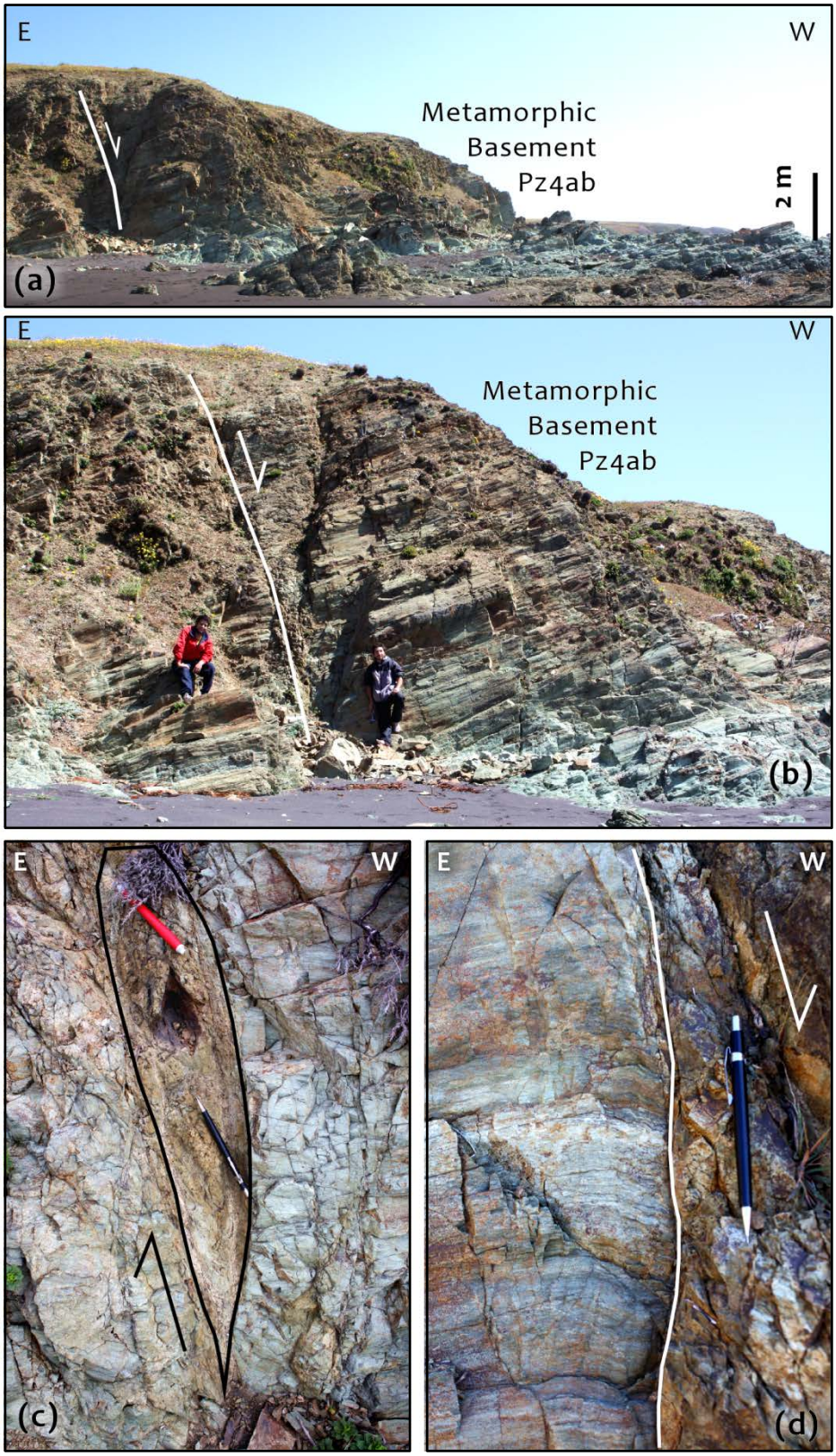

Figure DR13: (a) and (b) show outcrop of a NS-striking, W-dipping normal fault found at the coastal cliff in site 11 (Fig. 2, Table 1 and Section 4.1.4 in main manuscript). (c) and (d) are close ups of the fault zone showing kinematic indicators of normal displacement (sigmoid-shaped fabrics in the gouge and deflection of the schistosity in the foot-wall block).

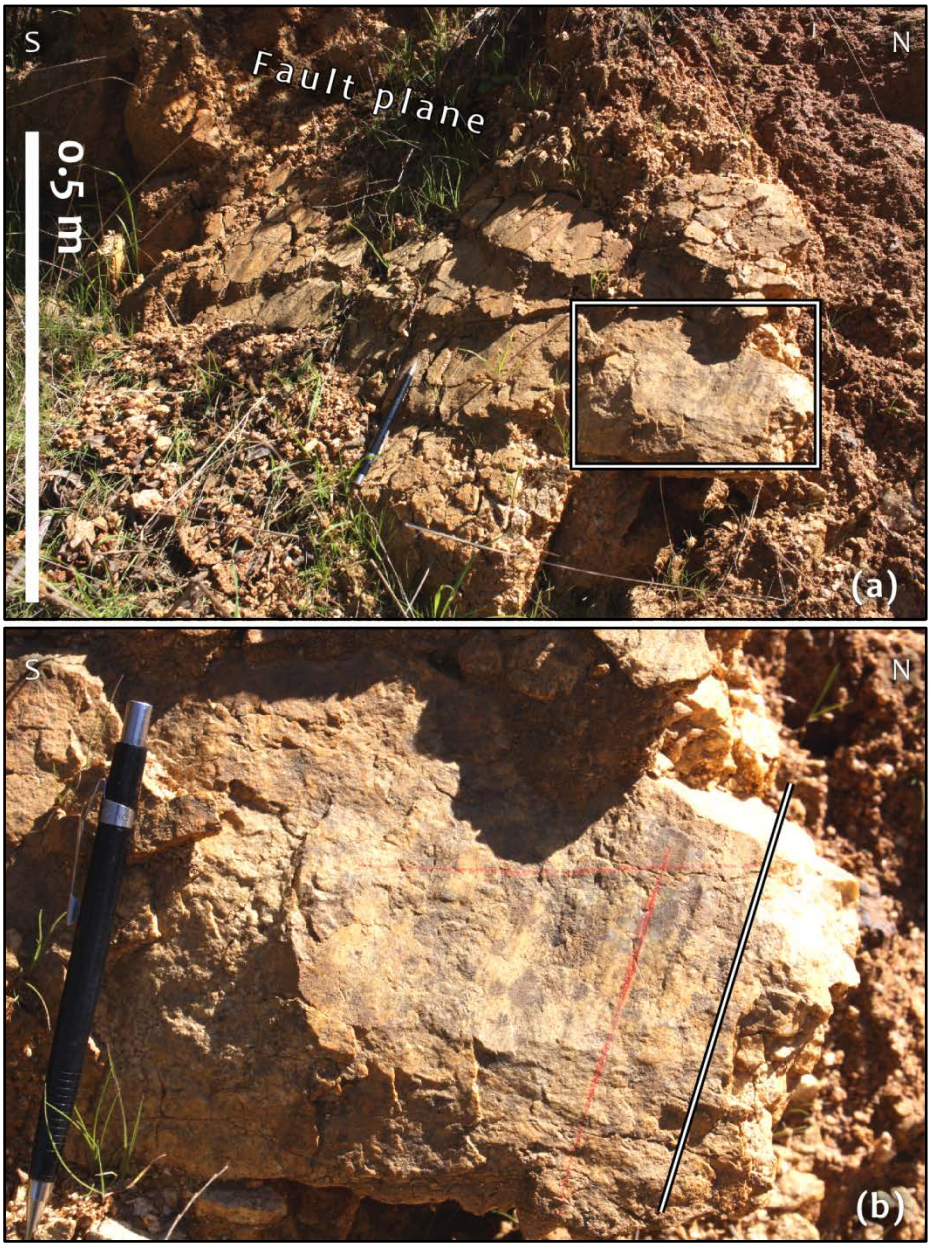

Figure DR14: (a) Outcrop of one of the normal faults found at the base of the Cáhuil-Vichuquén ridge scarp in site 14 (Fig. 2, Table 1 and Section 4.1.5 in main manuscript). (b) Close up to fault plane with slickensides. The structure affects the Paleozoic metamorphic basement rocks.

DR Section 2. Additional structural field examples of the Maule study region

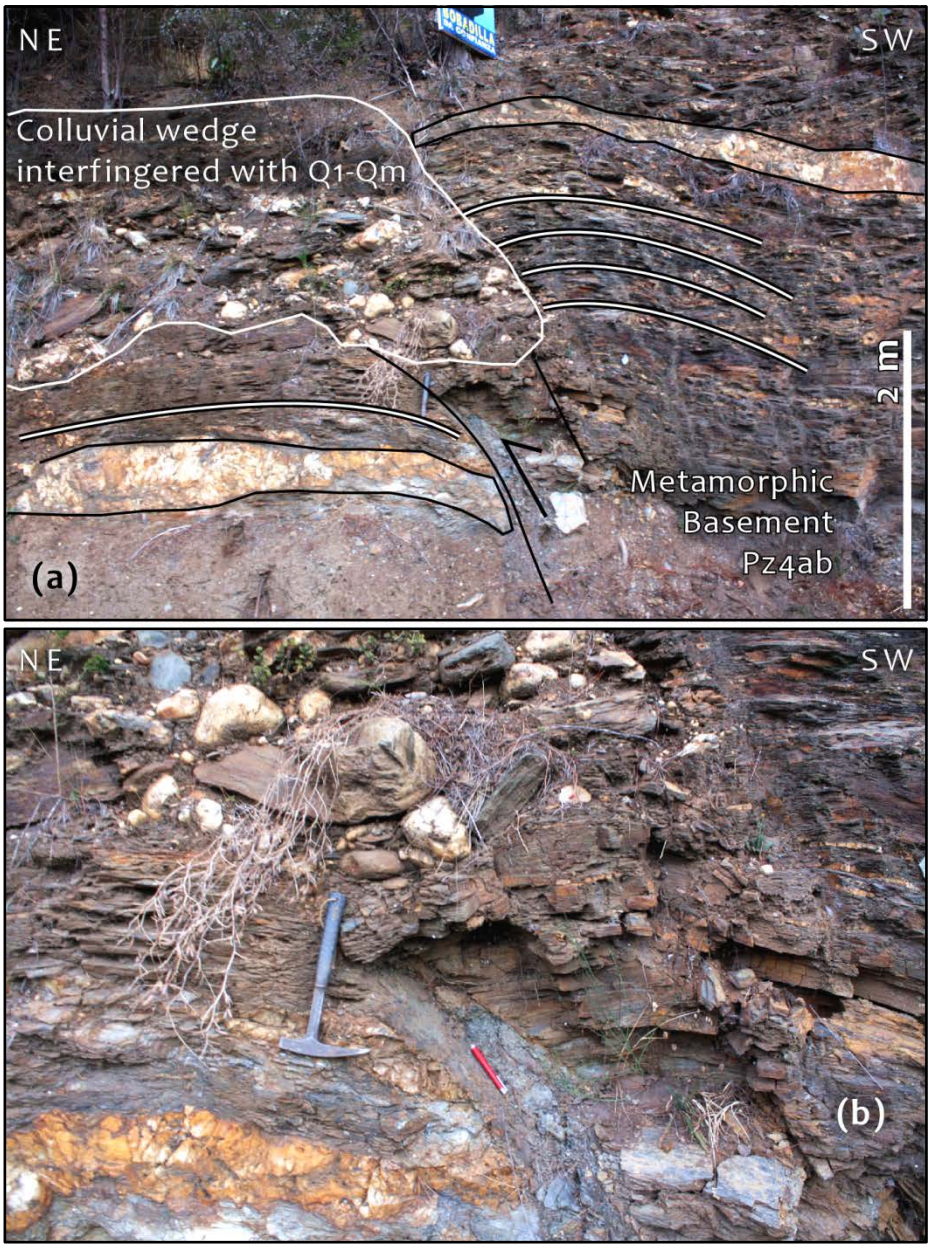

Figure DR15: (a) Color version of Figure 11 in main manuscript (site 20 in Fig.9and Table 2;Section 4.2.1 in main manuscript). (b) Close up to fault plane and colluvial wedge in the foot-wall. Outside the pictures to the left, the material of the wedge interfingers with Quaternary paleo-beach sedimentary rocks, which lie on top of a sub-horizontal abrasion platform cut on metamorphic basement rocks.

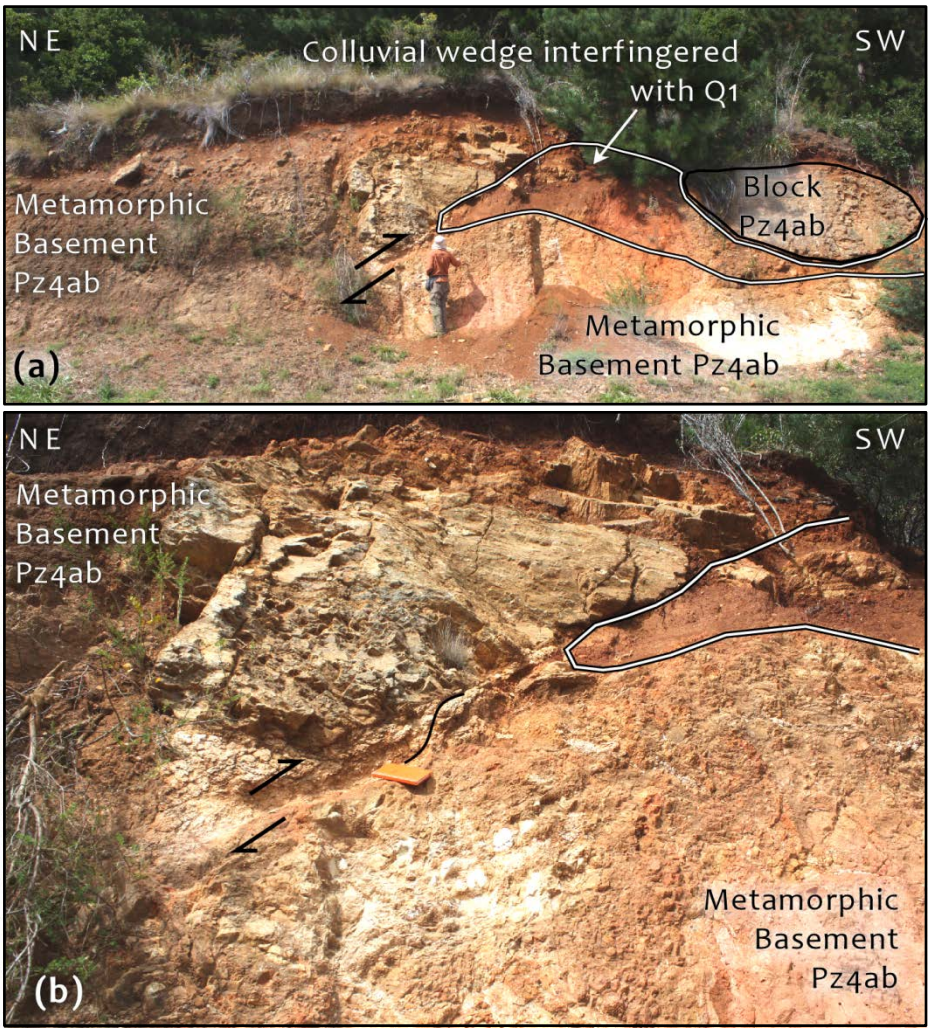

Figure DR16: (a) Outcrop of reverse fault found at site 21 affecting metamorphic rocks and Quaternary sedimentary units (Fig.9, Table 2 and Section 4.2.1 in main manuscript). Here the colluvial wedge in front of the scarp interfingers with Quaternary river deposits (Q1). (b) Close up to fault zone around the person at the center of picture in (a).

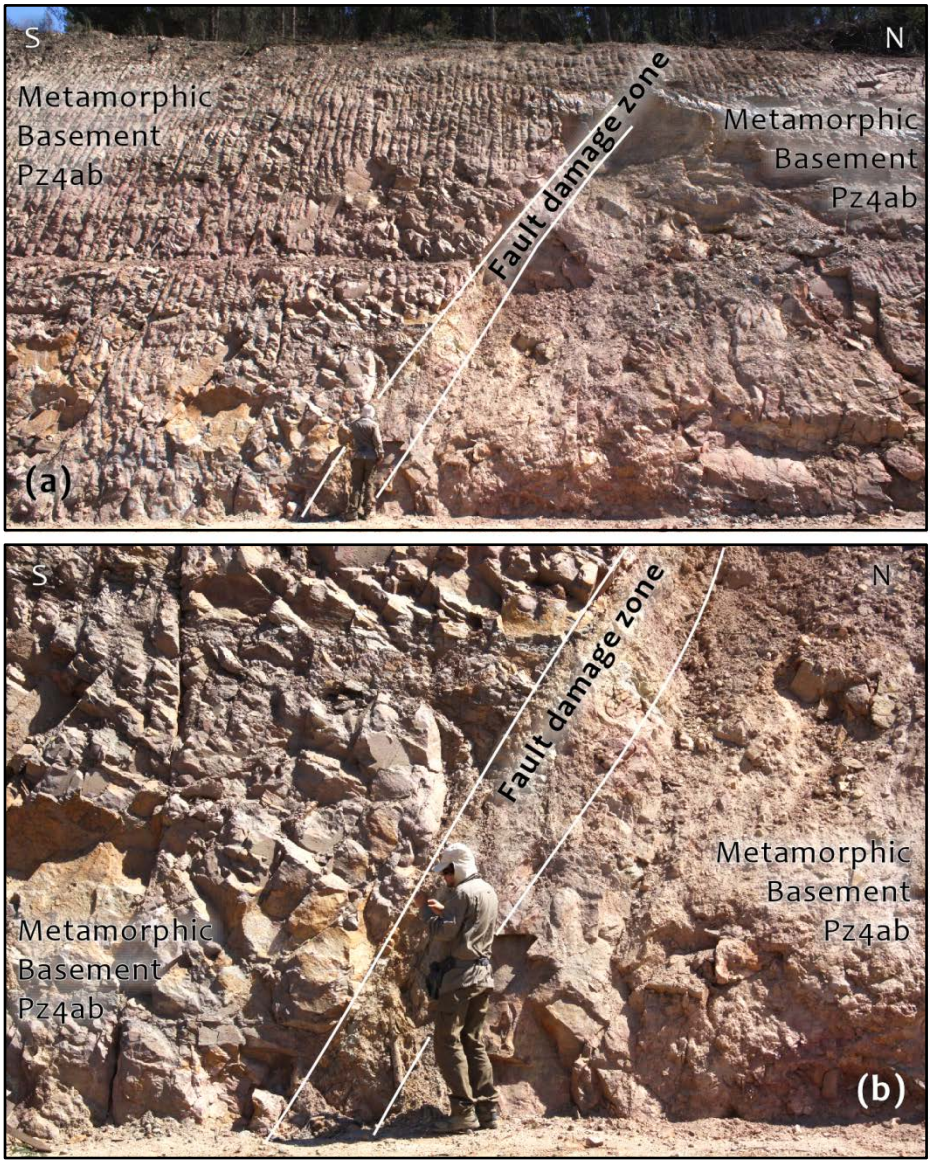

Figure DR17: (a) Outcrop of major fault affecting metamorphic basement at site 22 (Figs. 9-10, Table 2 and Section 4.2.2 in main manuscript). The width of the fault damage zone, as emphasized in the pictures, suggests a significant brittle deformation history accounted by this structure. (b) Close up around the location of the person at the lower center of photo (a).

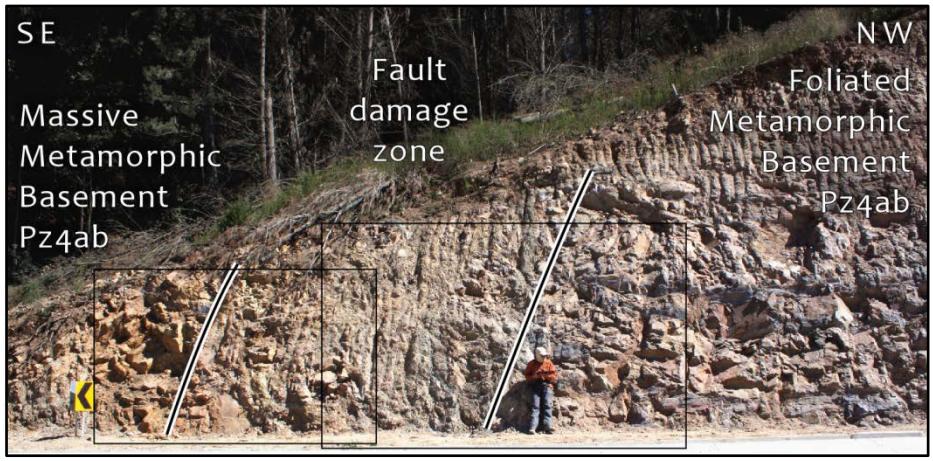

Figure DR18: Color version of Figure 12 in main manuscript (Fault 23a in Figs. 9-10 and Table 2; Section 4.2.2 in main manuscript). The boxes on the lower left and lower center of the picture show the location of Figs. DR19 and DR21 respectively.

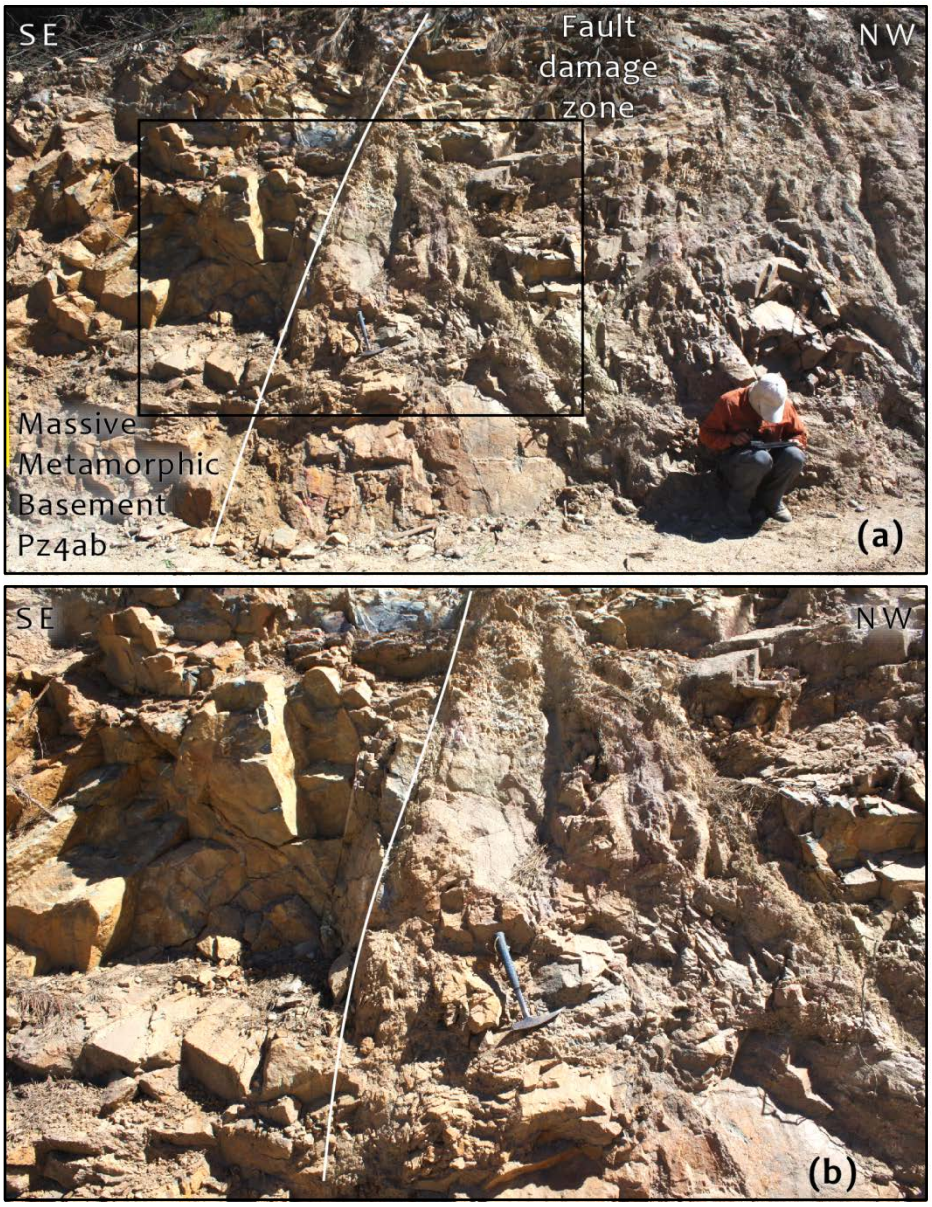

Figure DR19: (a) Contact between the top of the damage zone and the hanging-wall of the main fault in site 23 (location in Fig. DR20). (b) Close up to the black box in (a).

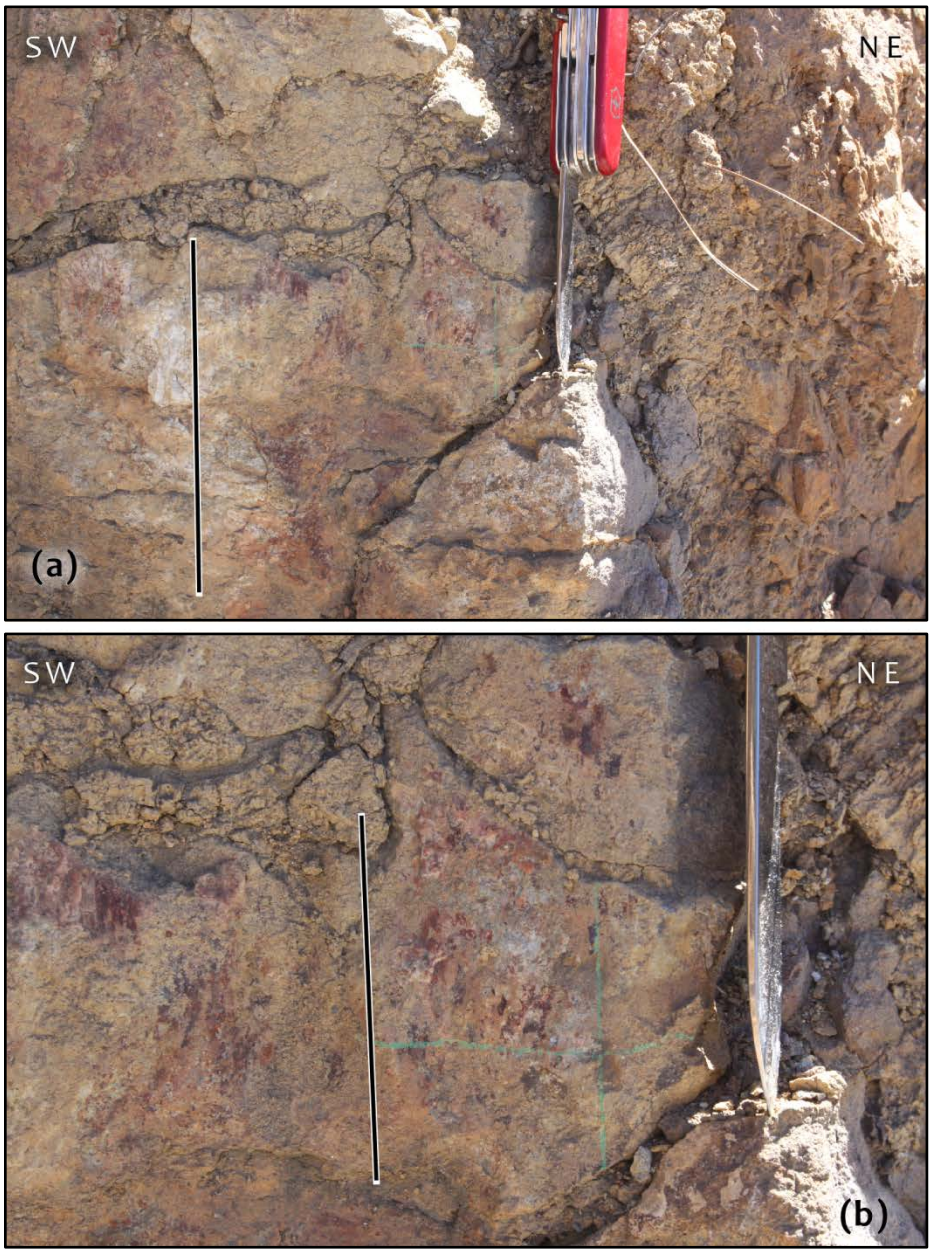

Figure DR20: (a) and (b) are close up views of a striated plane on the contact shown in Figure DR19.

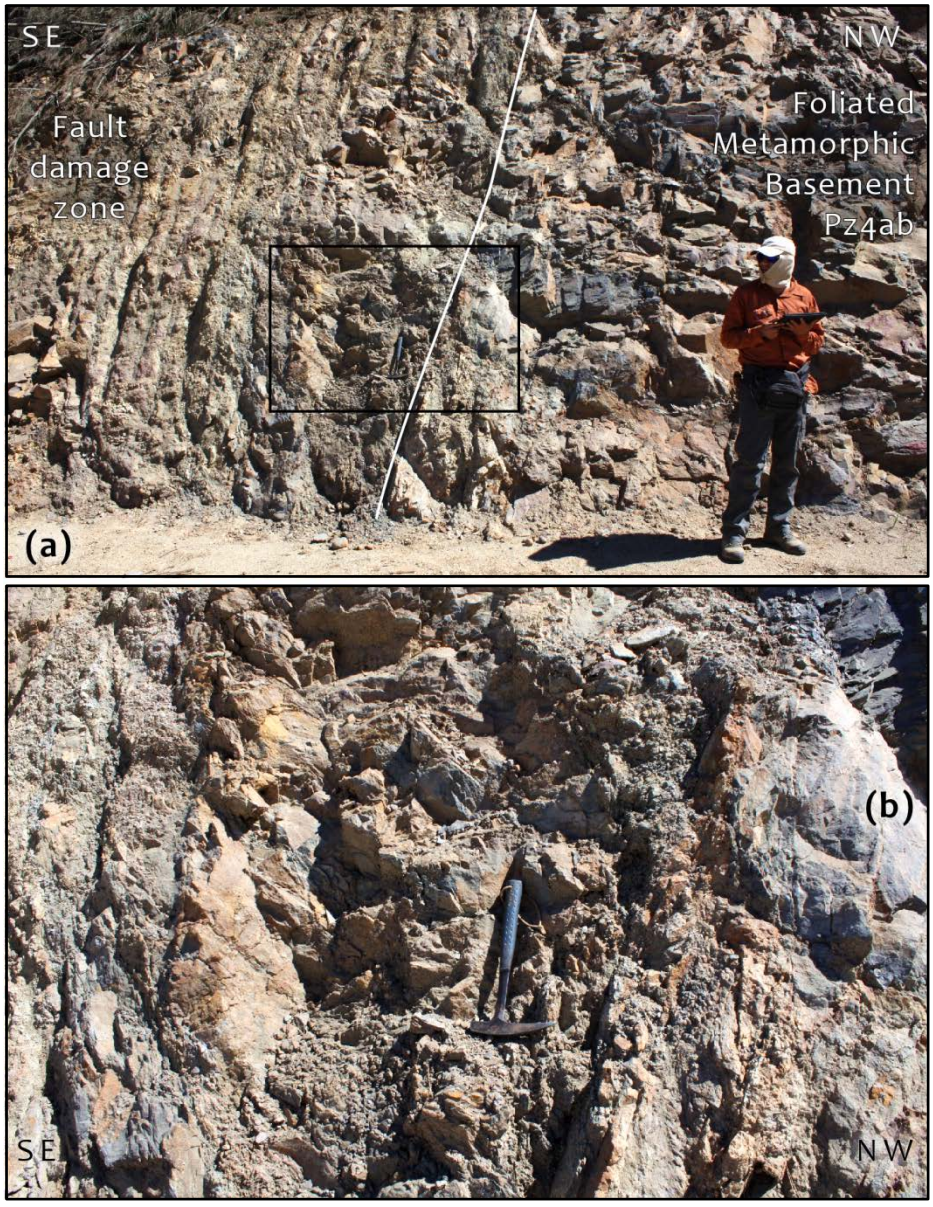

Figure DR21: (a) Contact between the bottom of the damage zone and the foot-wall of the main fault in site 23 (location in Fig. DR20). (b) Close up to the black box in (a).

Figure DR22: Outcrop of major normal fault bounding the scarp of the Maule ridge at site 29 (Figs. 9-10, Table 2 and Section 4.2.2 in main manuscript). The fault zone is bounded by the two white polygons illustrated on the right of the picture. The schistocity of the metamorphic basement in the hanging-wall is deflected close to the fault plane, as emphasized by the ornamentation, indicating normal sense of slip.

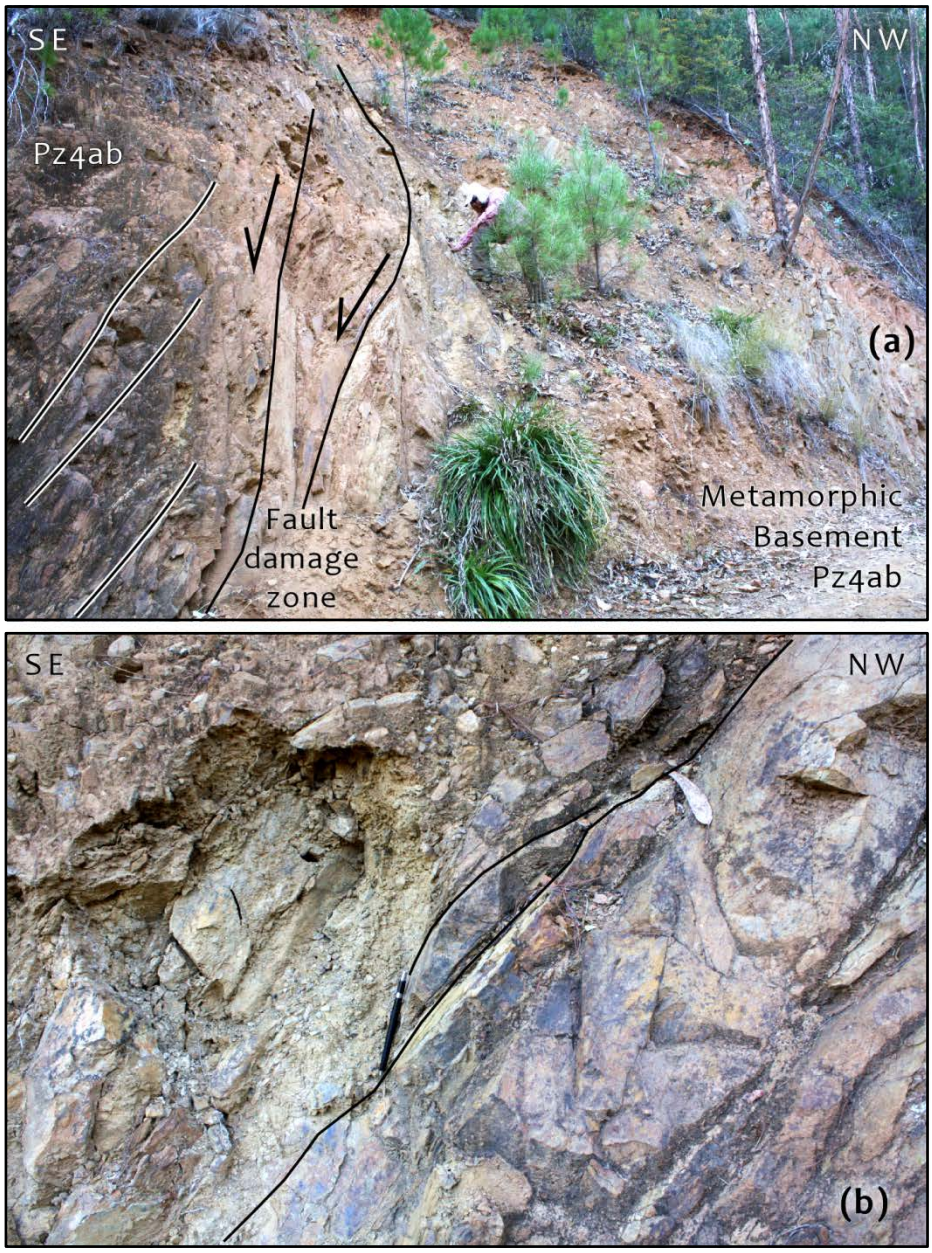

Figure DR23: (a) Outcrop of fault shown in Fig. DR22 emphasizing the damage zone of the structure (site 29 in Figs. 9-10 and Table 2; Section 4.2.2 in main manuscript). (b) Close up to the damage zone. Note that the fault gouge and breccia display sigmoid-shaped clasts which indicate shear slip of the structure.

DR Section 3. Infinitesimal 2D strain from GPS over the Maule earthquake rupture area

DR Section 3.1. Coseismic static surface displacements and first invariant of strain

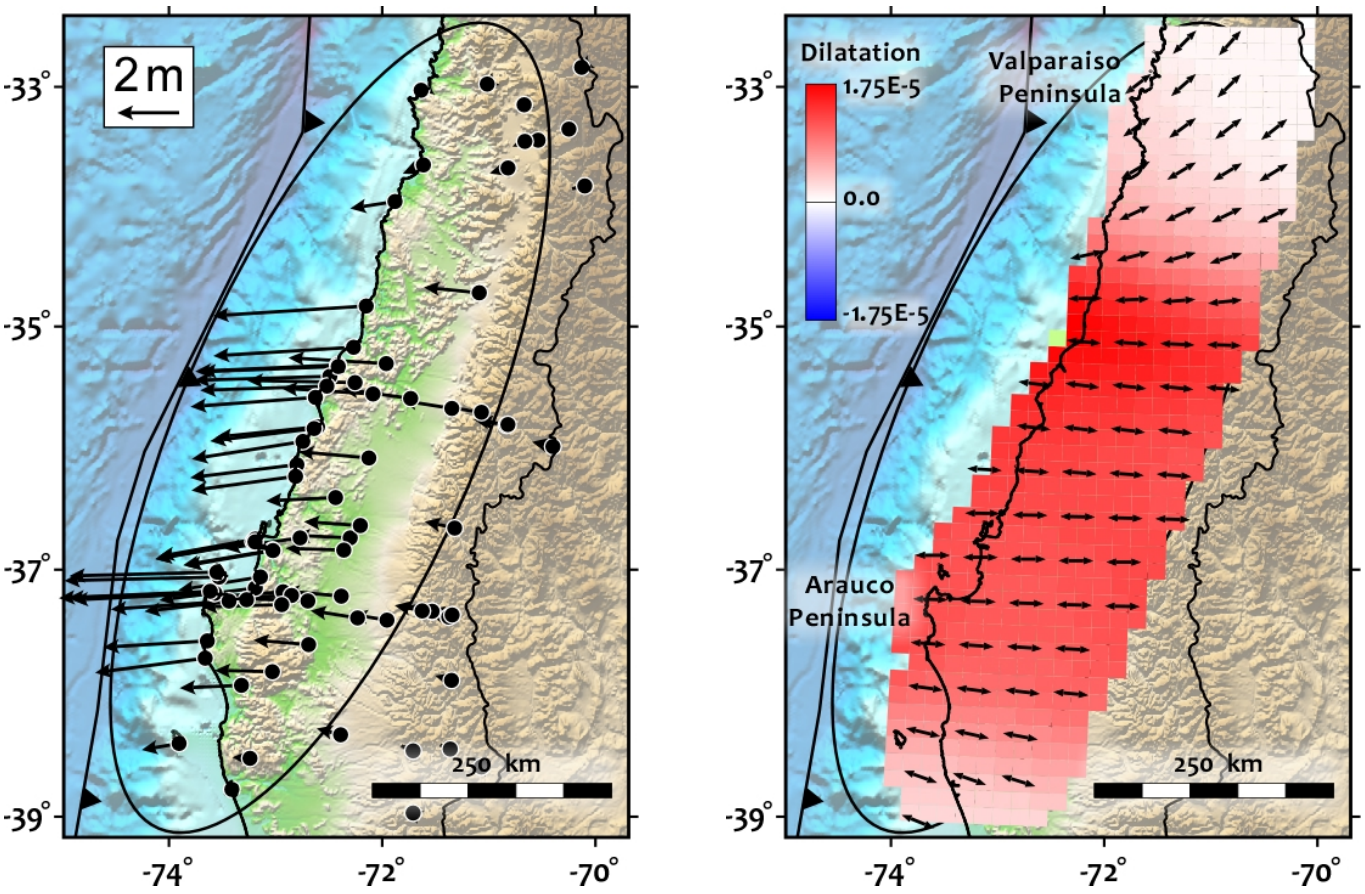

Figure DR24: Left, coseismic static surface GPS displacements generated by the subduction rebound of the 2010 Maule earthquake. GPS data from Vigny et al. (2011) and Moreno et al. (2012). Right, 2D infinitesimal strain calculated from these vectors capturing rapid coseismic positive dilatation (in red), caused by an excess of forearc extension. Black arrows represent the horizontal vector field of the principal extension strain (ε_3). See Section 5.2 and Figure 13 in main manuscript.

DR Section 3.1. Interseismic surface velocities and first invariant of strain

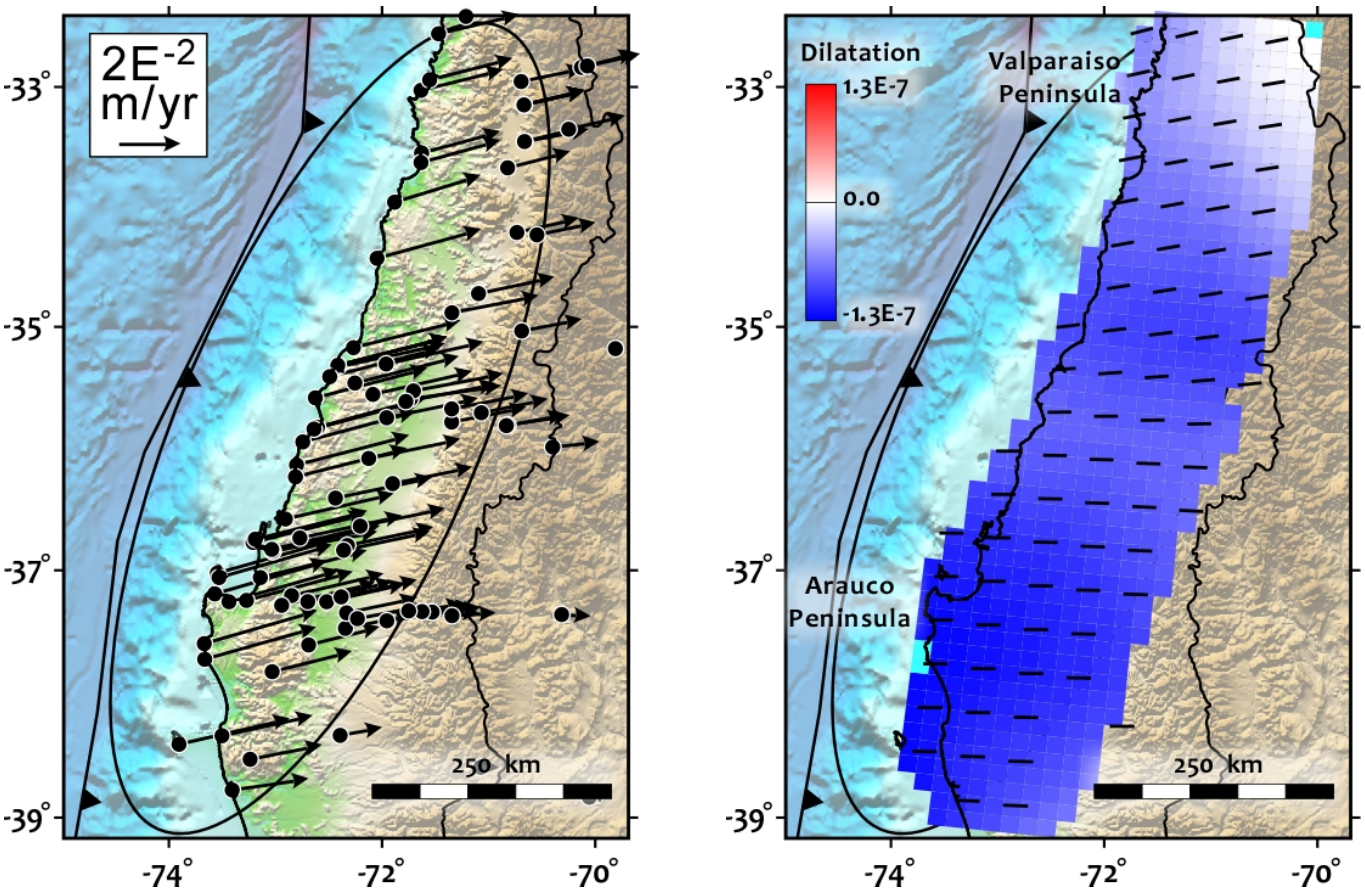

Figure DR25: Left, compilation of interseismic GPS velocities of the rupture area averaged between 1998 and February 2010, before the Maule earthquake. GPS data courtesy of Marianne Métois (Métois et al., 2012). The velocities before the megathrust show convergence-parallel inland motion of the upper plate. Right, slow shortening shown by the blue colors of the first invariant of strain dominates the interseismic period. Black lines represent the horizontal vector field of the principal shortening strain (ε_1). See Section 5.2 and Figure 13 in main manuscript.

References

Métois, M., Socquet, A., and Vigny, C., 2012, Interseismic coupling, segmentation and mechanical behavior of the central Chile subduction zone: Journal of Geophysical Research, v. 117, p. 16 PP., doi: 10.1029/2011JB008736.

Moreno, M., Melnick, D., Rosenau, M., Baez, J., Klotz, J., Oncken, O., Tassara, A., Chen, J., Bataille, K., Bevis, M., Socquet, A., Bolte, J., Vigny, C., Brooks, B., et al., 2012, Toward understanding tectonic control on the Mw 8.8 2010 Maule Chile earthquake: Earth and Planetary Science Letters, v. 321–322, p. 152–165, doi: 10.1016/j.epsl.2012.01.006.

Vigny, C., Socquet, A., Peyrat, S., Ruegg, J.-C., Métois, M., Madariaga, R., Morvan, S., Lancieri, M., Lacassin, R., Campos, J., Carrizo, D., Bejar-Pizarro, M., Barrientos, S., Armijo, R., et al., 2011, The 2010 Mw 8.8 Maule Megathrust Earthquake of Central Chile, Monitored by GPS: Science, v. 332, p. 1417–1421, doi: 10.1126/science.1204132.